ARTICLE IN PRESS

Available online at www.sciencedirect.com
SCIENCE DIRECT®

Chemical Physics Letters 403 (2005) 329–333

CHEMICAL PHYSICS LETTERS

www.elsevier.com/locate/cplett

# The inelastic neutron scattering spectra of α-3-amino-5-nitro-1,2,4-2H-triazole: Experiment and DFT calculations

Jennifer A. Ciezak *, S.F. Trevino

*Weapons and Materials Research Directorate, US Army Research Laboratory, Aberdeen Proving Ground, MD 21005, USA*
*NIST Center for Neutron Research, 100 Bureau Dr. MD 8562, Gaithersburg, MD 20899, USA*

Received 7 December 2004; in final form 10 January 2005

**Abstract**

The inelastic neutron scattering (INS) spectrum of α-3-amino-5-nitro-1,2,4-triazole is presented through 1200 $cm^{-1}$. A comparison of the INS spectrum with an isolated molecule B3LYP/6-311G** calculation reveals generally good frequency and intensity agreement with two notable differences in intensity. Periodic density functional theory (DFT) calculations are employed to determine whether the intermolecular hydrogen bonding is the origin of these differences between the B3LYP/6-311G** and INS spectrum.


## 1. Introduction

The solid energetic compound, 3-amino-5-nitro-1,2,4-2H-triazole (ANTA) shown in Fig. 1, is employed in a wide range of applications from blasting agents to explosive welding because of its extraordinary stability under thermal, impact, or shock initiating conditions. As with any energetic material, a primary concern is safety, as there is always a finite chance of accidental ignition or initiation [1]. To address safety concerns, researchers have focused on developing a deeper understanding of the chemical and physical processes leading to detonation [2–4]. It is widely thought that shock compression results from energy transfer from the phonons to the internal degrees of freedom of a molecule [2,5–7]. Thus, the vibrational properties of both the crystalline lattice and the internal molecular vibrations play an important role in this process. A clear need exists for detailed characterization of the internal molecular vibrations of explosive materials using both experimental vibrational spectroscopy and ab inito methods.

ANTA is known to exist in two polymorphic crystalline phases. The α-phase contains eight molecules per unit cell in a monoclinic lattice with C2/c symmetry and is hydrogen bonded into twisted ribbons [8]. The β-phase contains four molecules per unit cell with $P2_1/n$ symmetry and has extended planar molecular sheets [9]. The presence of an intermolecular hydrogen bonding network likely plays an important role in the insensitivity and stability of ANTA. In the case of a similar insensitive explosive, TATB, strong intramolecular hydrogen bonds are thought to result in the great stability [10].

The interest in the INS vibrational spectrum stems in part from previous vibrational theoretical work of α-ANTA [11] done on an isolated molecule at several theory levels. In this 1998 study, no experimental vibrational data was available to make a conclusion as to the adequacy of the calculations. In addition, solid-state DFT calculations have become more popular and generally show better agreement with experimental results than isolated molecule calculations because of the

* Corresponding author. Fax: +1 301 921 9847.
*E-mail address:* jciezak@arl.army.mil (J.A. Ciezak).

0009-2614/$ - see front matter © 2005 Elsevier B.V. All rights reserved.
doi:10.1016/j.cplett.2005.01.033

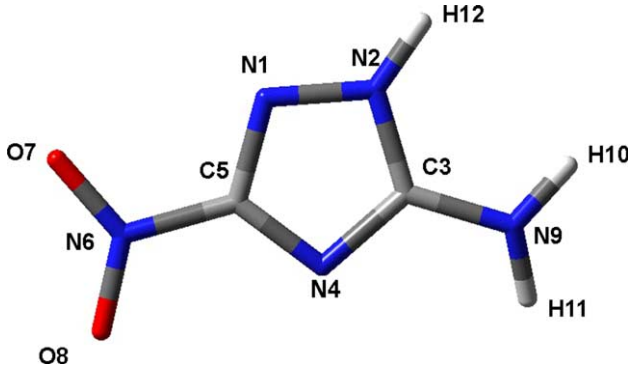


Fig. 1. The molecular structure and numbering scheme for α-ANTA.

inclusion of the intermolecular interactions. We have used INS spectroscopy to obtain the low-frequency vibrations of α-ANTA. In addition, we have performed solid-state calculations to examine the crystal effects on the structure and vibrations of α-ANTA. INS spectroscopy is particularly useful as a vibrational spectroscopic method when investing the molecular dynamics of organic hydrocarbons because of its immense sensitivity to hydrogen atom motions. The vibrational intensity is proportional to the contribution of hydrogen motion that constitutes a normal mode. This makes the calculation of an INS spectrum quite simple, permitting a detailed test of a proposed description of the atomic dynamics by comparison with experiment [12].

## 2. Methods

The INS experiment was carried out at the NIST Center for Neutron Research [13] using the Filter Analyzer Neutron Spectrometer (FANS) located at BT-4. The vibrational spectrum was recorded over the 110–1200 $cm^{-1}$ energy range. Extensive details of neutron scattering in general and instrumental design is available [12]. The DAVE program was used to normalize the experimental spectrum with respect to the background [14].

The INS measurements were performed on a polycrystalline sample of ca. 1 g of α-ANTA held at 25 K. The sample was obtained from Picatinny Arsenal and used without further purification. The synthesis of α-ANTA is discussed in [1].

An isolated molecule geometry optimization and normal mode analysis was performed using GAUSSIAN 03 [15]. The B3LYP [16] hybrid functional was used with the 6-311G** basis set. Tight convergence criteria was used. A solid-state geometry optimization and frequency calculation was done using DMol3 [17,18] on the SGI Origin Array at the Aeronautical Systems Major Shared Resource Center. The α-ANTA crystal structure for the solid-state DFT calculation was taken from [8]. The dnd numerical basis set and BLYP GGA functional [19] were

Table 1
Bond lengths for the crystallographic, isolated molecule, and solid-state DFT α-ANTA geometries

| Bond | BLYP dnd | B3LYP 6-311G** | B3LYP 6-31G** [11] | B3LYP 6-311+G** [11] | MP2 6-31G** [11] | MP2 6-311G** [11] | MP2 6-311+G** [11] | BLYP 6-31G** [11] | BLYP 6-311+G** [11] | Exp [8] |
|---|---|---|---|---|---|---|---|---|---|---|
| N1–N2 | 1.3690 | 1.3631 | 1.3615 | 1.3594 | 1.3581 | 1.3538 | 1.3541 | 1.3787 | 1.3763 | 1.3687 |
| N2–C3 | 1.3770 | 1.3484 | 1.3633 | 1.3625 | 1.3589 | 1.3588 | 1.3592 | 1.3783 | 1.3777 | 1.3499 |
| C3–N4 | 1.3470 | 1.3435 | 1.3237 | 1.3204 | 1.3298 | 1.3270 | 1.3285 | 1.3373 | 1.3335 | 1.3336 |
| N4–C5 | 1.3520 | 1.3108 | 1.3545 | 1.3521 | 1.3529 | 1.3514 | 1.3520 | 1.3673 | 1.3641 | 1.3439 |
| C5–N1 | 1.3280 | 1.3198 | 1.3171 | 1.3116 | 1.3345 | 1.3303 | 1.3308 | 1.3355 | 1.3293 | 1.3085 |
| C5–N6 | 1.4480 | 1.4519 | 1.4619 | 1.4689 | 1.4523 | 1.4589 | 1.4573 | 1.4756 | 1.4829 | 1.4467 |
| N6–O7 | 1.2450 | 1.2216 | 1.2275 | 1.2210 | 1.2415 | 1.2285 | 1.2310 | 1.2479 | 1.2418 | 1.2256 |
| N6–O8 | 1.2500 | 1.2236 | 1.2275 | 1.2202 | 1.2414 | 1.2285 | 1.2310 | 1.2468 | 1.2410 | 1.2205 |
| C3–N9 | 1.3470 | 1.3682 | 1.3721 | 1.3693 | 1.3830 | 1.3830 | 1.3825 | 1.3843 | 1.3803 | 1.3408 |
| N9–H10 | 1.0340 | 1.0080 | 1.0110 | 1.0093 | 1.0106 | 1.0117 | 1.0123 | 1.0199 | 1.0173 | 0.8819 |
| N9–H11 | 1.0230 | 1.0078 | 1.0115 | 1.0101 | 1.0109 | 1.0121 | 1.0127 | 1.0200 | 1.0180 | 0.8743 |
| N2–H12 | 1.0300 | 1.0092 | 1.0095 | 1.0091 | 1.0087 | 1.0101 | 1.0112 | 1.0179 | 1.0172 | 0.8437 |

used. All B3LYP/6-311G** modes were scaled by 0.987 to improve agreement with the INS results. The solid-state BLYP/dnd results are unscaled.

The calculated INS spectrum of α-ANTA was constructed using the A-Climax program v.5.1.3 [20]. Combination and overtone vibrations to four quanta are included. The Sachs–Teller mass tensor was used providing each scattering atom with its own effective mass [21].

## 3. Results and discussion

### 3.1. Molecular geometry

The calculated α-ANTA bond lengths from this study and those previously reported [11] are provided with the α-polymorph crystallographic bond lengths in Table 1. The majority of the bond lengths predicted with the Gaussian-type methods are longer than the corresponding crystallographic values. The primary exception is the N1–N2 bond where the majority of the calculated bond lengths are shorter. The B3LYP/6-311G** bond lengths differ from the α-ANTA crystal averages with an rms deviation of 0.0726 Å. This rms value is very similar to the previously reported rms values using the B3LYP/6-31G** (0.0735 Å) and B3LYP/6-311+G** (0.0729 Å) levels of theory. The rms values for BLYP/6-31G** and BLYP/6-311+G** levels of theory are 0.0800 and 0.0787 Å, respectively.

The deviations from the experimental bond lengths are generally larger using MP2 theory. Rice and Chabalowski [22] also observed this trend while performing similar calculations on RDX. The rms values are 0.0741 Å at the MP2/6-31G** level, 0.0744 Å at the MP2/6-311G** level and 0.0748 Å using the MP2/6-311+G** level of theory.

The rms deviation for the solid-state DMol3 BLYP/dnd geometry optimization is, at 0.0830 Å, large relative to the Gaussian basis set calculations. An overall lengthening of the bonds is observed in the solid-state calculation. A much larger twist of the $NH_2$ group is found in the BLYP/dnd results, most likely due to the small distortion caused by the hydrogen bonding network.

### 3.2. Molecular normal mode analysis

The experimental INS spectrum of α-ANTA recorded on FANS is shown in Fig. 2. The A-Climax simulated INS spectra at both the B3LYP/6-311G** and BLYP/dnd levels of theory is presented in Fig. 2. It is clear that there is generally good agreement both in frequency and intensity between the experimental and theoretical INS spectra. Combinations and overtone vibrations are observed in the INS spectrum at ca. 274, 347, 476, 564, 621, 677, 790, 879 and 904 $cm^{-1}$. The corresponding theoretical vibrations reproduce the experimental results well.

The resolvable INS and corresponding calculated normal modes are listed in Table 2. Approximate descriptions of the normal modes are given. Our assignments agree with those previously reported with the exception of the $NH_2$ deformation of $\nu 11$, which was previously ascribed to $\nu 12$. In a number of cases, the B3LYP/6-311G** normal mode frequencies differ from

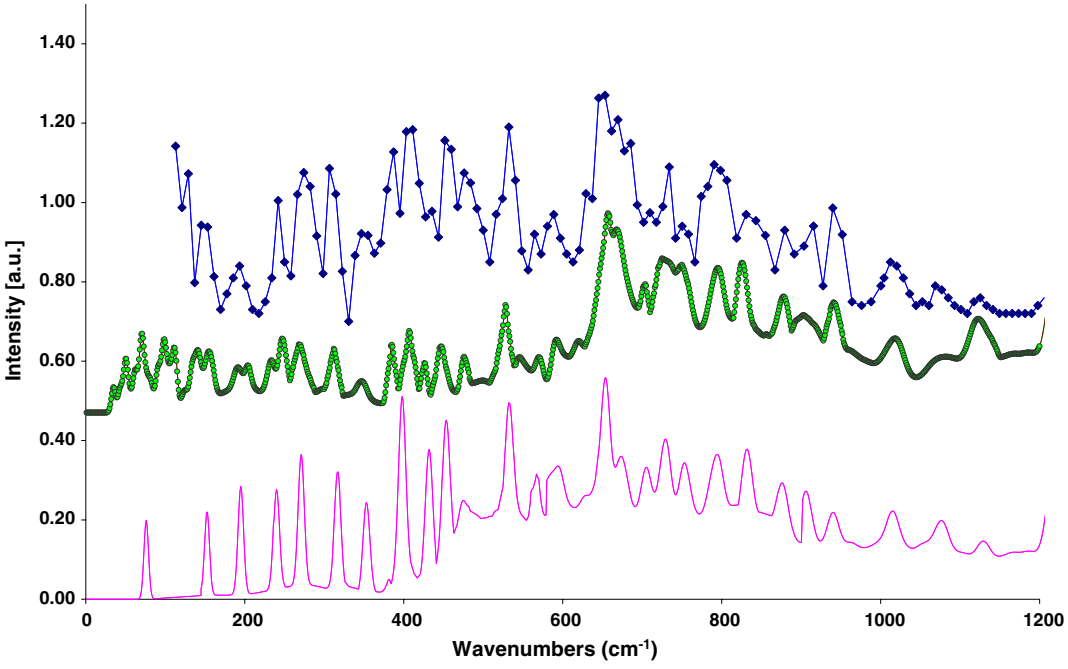


Fig. 2. The INS spectrum (diamond), simulated BLYP/dnd (circle) and B3LYP/6-311G** (gray) from ca. 0 to 1200 $cm^{-1}$. Spectra have been scaled for clarity.

Table 2
INS and DFT molecular vibrational modes for the ca. 25–3550 $cm^{-1}$ region of the α-ANTA spectrum

| INS ($cm^{-1}$) | BLYP dnd | B3LYP 6-311G** | B3LYP 6-31G** [11] | B3LYP 6-311+G** [11] | MP2 6-31G* [11] | MP2 6-311G** [11] | MP2 6-311+G** [11] | BLYP 6-31G** [11] | BLYP 6-311+G** [11] | Assignment | Mode |
|---|---|---|---|---|---|---|---|---|---|---|---|
| | 51 | 77 | 42 | 33 | 27 | 24 | 41 | 45 | 33 | $NO_2$ torsion | *v*1 |
| 145 | 143 | 153 | 163 | 161 | 153 | 159 | 150 | 160 | 158 | Skeletal deformation | *v*2 |
| 193 | 193 | 196 | 198 | 197 | 191 | 94 | 192 | 196 | 195 | $NO_2$ rock | *v*3 |
| 242 | 248 | 241 | 258 | 253 | 207 | 211 | 205 | 266 | 260 | $NH_2$ rock | *v*4 |
| 307 | 313 | 317 | 329 | 326 | 308 | 319 | 301 | 322 | 320 | Skeletal deformation | *v*5 |
| 387 | 386 | 380 | 375 | 374 | 366 | 369 | 370 | 371 | 370 | Ring deformation | *v*6 |
| 411 | 407 | 398 | 415 | 411 | 409 | 413 | 408 | 406 | 403 | C–$NO_2$ deformation | v7 |
| 451 | 448 | 455 | 479 | 485 | 500 | 485 | 455 | 451 | 459 | $NO_2$ deformation | *v*8 |
| 533 | 529 | 533 | 540 | 539 | 525 | 534 | 517 | 534 | 533 | $NH_2$ deformation | *v*9 |
| 588 | 593 | 596 | 582 | 548 | 608 | 618 | 620 | 605 | 560 | Ring torsion + $NO_2$ deformation | *v*10 |
| 669 | 670 | 676 | 634 | 634 | 636 | 648 | 635 | 625 | 625 | Ring torsion + $NH_2$ def. | *v*11 |
| 710 | 705 | 708 | 708 | 710 | 680 | 704 | 701 | 697 | 697 | Ring + $NO_2$ def. | *v*12 |
| 734 | 726 | 730 | 723 | 723 | 693 | 719 | 706 | 719 | 718 | Ring torsion | *v*13 |
| 750 | 751 | 755 | 749 | 755 | 726 | 747 | 730 | 729 | 737 | Ring torsion | *v*14 |
| 831 | 827 | 834 | 818 | 825 | 784 | 812 | 808 | 800 | 806 | $NO_2$ def + ring def | *v*15 |
| 940 | 944 | 942 | 982 | 980 | 950 | 963 | 961 | 966 | 965 | N4–C5–N1 bend | *v*16 |
| 1012 | 1020 | 1017 | 1009 | 1003 | 1002 | 1011 | 1010 | 998 | 991 | N1–N2–C3 bend | *v*17 |
| 1069 | 1078 | 1079 | 1077 | 1070 | 1076 | 1082 | 1079 | 1071 | 1062 | Ring deformation | *v*18 |
| 1125 | 1124 | 1131 | 1124 | 1117 | 1143 | 1159 | 1157 | 1095 | 1088 | N–N symmetric stretch | *v*19 |
| | 1249 | 1269 | 1299 | 1288 | 1258 | 1274 | 1268 | 1272 | 1255 | $NO_2$ symmetric stretch | *v*20 |
| | 1310 | 1310 | 1308 | 1299 | 1286 | 1291 | 1287 | 1289 | 1278 | Ring def + N–H bend | v21 |
| | 1339 | 1348 | 1368 | 1341 | 1373 | 1379 | 1375 | 1305 | 1285 | C–$NO_2$ symmetric stretch | *v*22 |
| | 1387 | 1389 | 1414 | 1400 | 1402 | 1410 | 1404 | 1389 | 1376 | Ring deformation | *v*23 |
| | 1485 | 1483 | 1494 | 1482 | 1451 | 1462 | 1453 | 1452 | 1438 | C–N symmetric stretch | *v*24 |
| | 1526 | 1536 | 1553 | 1544 | 1535 | 1535 | 1531 | 1521 | 1470 | C–$NH_2$ asym. + $NH_2$ bend | *v*25 |
| | 1585 | 1589 | 1600 | 1554 | 1595 | 1594 | 1590 | 1550 | 1542 | C–$NH_2$ symm. stretch + $NH_2$ bend | *v*26 |
| | 1669 | 1665 | 1617 | 1606 | 1702 | 1722 | 1699 | 1612 | 1605 | N–O asymm. stretch | *v*27 |
| | 3409 | 3442 | 3438 | 3436 | 3396 | 3407 | 3405 | 3442 | 3450 | N–H stretch NH2 | *v*28 |
| | 3482 | 3501 | 3517 | 3498 | 3485 | 3490 | 3480 | 3519 | 3505 | N–H stretch (N1–H12) | *v*29 |
| | 3545 | 3550 | 3543 | 3533 | 3504 | 3507 | 3506 | 3547 | 3547 | N–H asymm. stretch (NH2) | *v*30 |

the experimental values by less than 10 $cm^{-1}$. The rms deviation for the B3LYP/6-311G** level of theory is 6.4 $cm^{-1}$. The rms deviations at the B3LYP/6-31G** and B3LYP/6-311+G** levels of theory are 17.4 and 19.5 $cm^{-1}$, respectively. Rms deviations of 19.9 and 20.4 $cm^{-1}$ were found at the BLYP/6-31G** and BLYP/6-311+G** theory levels. Similar to what was observed in the calculated geometries, larger rms deviations are observed with the MP2 results. A rms deviation of 25.4 $cm^{-1}$ was found using MP2/6-31G**. The rms deviation at the MP2/6-311G** level was 30.2 $cm^{-1}$, while the MP2/6-311+G** level had an rms value of 30.5 $cm^{-1}$. The degree of frequency and intensity agreement between the B3LYP/6-311G** and experimental frequencies is noteworthy considering the presence of hydrogen bonds and the relatively large rms values of the other levels of theory.

It seems necessary to mention two instances in the B3LYP/6-311G** spectrum shown in Fig. 2, where the intensities of the vibrations are considerably underestimated. The first concerns the ring deformation ($v6$) predicted at 380 $cm^{-1}$. Given the large crystal size ($Z = 8$), it is easy to suggest that the large intensity in the experimental spectrum stems from a collective vibration in the crystal. This discrepancy between the B3LYP/6-311G** and experimental spectrum results from an insufficient model. The second discrepancy in intensity is noted ca. 676 $cm^{-1}$ in the B3LYP/6-311G** spectrum. The vibrational mode is the result of the out-of-plane bend of the N–H hydrogen bond. Again, our isolated molecule model does not give an accurate representation of this vibration due to lack of intermolecular interactions.

The normal modes of the solid-state BLYP/dnd calculations are provided in Table 2. It is easy to see the excellent agreement between both the frequencies and intensities by looking at Table 2 and Fig. 2. The rms deviation is 4.7 $cm^{-1}$. The generally small frequency differences can be attributed to the differences between the room temperature and 15 K unit cell lattice constants. The intensities of $v6$ and $v11$ are more adequately reproduced using the solid-state methods. The better intensity agreement indicates the necessity of using a full-periodic representation to obtain an accurate representation of the vibrational dynamics. Optical spectroscopic studies are expected to provide the required information to complete the vibrational analysis of α-ANTA and we hope this report will stimulate them.

## Acknowledgements

The NIST Center for Neutron Research is thanked for neutron beam access on the FANS instrument. This work was supported the Army Research Laboratory. J.C. was supported by a National Research Council Fellowship with the Army Research Laboratory during the course of this research. Picatinny Arsenal at ARDEC is thanked for the sample of ANTA.

## References

[1] K.-Y. Lee, M.D. Coburn, M.A. Hiskey, Los Alamos National Laboratory Report, LA-12582-MS, June 1993.
[2] K.L. McNesby, C.S. Coffey, J. Phys. Chem. B 101 (1997) 3097.
[3] Y.A. Gruzdkov, Y.M. Gupta, J. Phys. Chem. A 105 (2001) 6197.
[4] H.V. Brand, R.L. Rabie, D.J. Funk, I. Diaz-Acosta, P. Pulay, T.K. Lippert, J. Phys. Chem. B 106 (2002) 10594.
[5] D.D. Dlott, M.D. Fayer, J. Chem. Phys. 92 (1990) 3798.
[6] A. Tokmanoff, M.D. Fayer, D.D. Dlott, J. Phys. Chem. 97 (1993) 1901.
[7] C.M. Tarver, J. Phys. Chem. A 101 (1997) 4845.
[8] E. Garcia, K.-Y. Lee, Acta Cryst. C 48 (1992) 1682.
[9] K.-Y. Lee, R. Gilardi, M.A. Hiskey, J.R. Stine, Mater. Res. Soc. Symp. Proc. 418 (1996) 43.
[10] B.M. Dobratz, The Insensitive High Explosive TATB: Development and Characterization-1888 to 1994, Los Alamos Nat. Lab, Los Alamos, NM, 1995.
[11] D.C. Sorescu, C.M. Bennett, D.L. Thompson, J. Phys. Chem. A 102 (1998) 10357.
[12] B.S. Hudson, J. Phys. Chem. A 105 (2001) 3949.
[13] Certain commercial software, instruments and materials are identified in this paper to foster understanding. Such identification does not imply recommendation or endorsement by the National Institutes of Standard and Technology, nor does it imply that the materials or equipment identified are necessarily the best available for the purpose..
[14] R. Azuah, C. Brown, J. Copley, R. Dimeo, S.-H. Lee, A. Munter, S. Park, Y. Qui, Data Analysis and Visualization Environment (DAVE) v. 1.2.
[15] M.J. Frisch et al., GAUSSIAN 03 (Revision B.03), Gaussian, Inc., Pittsburgh, PA, 2003.
[16] The B3LYP functional is Becke's three parameter hybrid method with LYP correlation functional A.D. Becke, J. Chem. Phys. 98 (1993) 5648.
[17] B. Delley, J. Chem. Phys. 113 (2003) 7756.
[18] B. Delley, J. Chem. Phys. 92 (1990) 508.
[19] A.D. Becke, J. Chem. Phys. 88 (1988) 2547.
[20] A.J. Ramirez-Cuesta, Comput. Phys. Commun. 157 (2004) 226.
[21] J. Tomkinson, G.J. Kearley, Nucl. Instrum. Meth. Phys. Res. A 354 (1995) 169.
[22] B.M. Rice, C.F. Chabalowski, J. Phys. Chem. A 101 (1997) 8720.